Applied Physics Letters

Continuously graded doped semiconducting polymers enhance thermoelectric cooling

Cite as: Appl. Phys. Lett. **119**, 013902 (2021); https://doi.org/10.1063/5.0055634
Submitted: 30 April 2021 • Accepted: 11 June 2021 • Published Online: 06 July 2021

Tengzhou Ma, William Kent, Ban Xuan Dong, et al.

Applied Physics Letters ARTICLE scitation.org/journal/apl

Continuously graded doped semiconducting polymers enhance thermoelectric cooling

Cite as: Appl. Phys. Lett. **119**, 013902 (2021); doi: 10.1063/5.0055634
Submitted: 30 April 2021 · Accepted: 11 June 2021 ·
Published Online: 6 July 2021

View Online Export Citation CrossMark

Tengzhou Ma, William Kent, Ban Xuan Dong, Garrett L. Grocke, and Shrayesh N. Patel[a)]

AFFILIATIONS

Pritzker School of Molecular Engineering, University of Chicago, 5640 S Ellis Ave, Chicago, Illinois 60637, USA

Note: This paper is part of the APL Special Collection on Organic and Hybrid Thermoelectrics.
[a)]**Author to whom correspondence should be addressed:** shrayesh@uchicago.edu

ABSTRACT

Spatial control of thermoelectric (TE) material properties through functional grading is a promising strategy in improving cooling performance. Notably, studies on organic-based functionally graded materials for thermoelectrics have been limited compared to their inorganic-based counterparts. In this Letter, we demonstrate how the inherent processability of semiconducting polymers coupled with molecular doping provides a facile approach in fabricating continuously graded (CG) thin films beneficial for thermoelectric (Peltier) cooling. We achieve CG thin films with 1D profiles in conductivity (σ) and Seebeck coefficient (α) through spatial compositional control of the molecular *p*-dopant 2,3,5,6-tetrafluoro-7,7,8,8-tetracyanoquinodimethane in semiconducting poly[2,5-bis(3-tetradecylthiophen-2-yl) thieno [3,2-b]thiophene]. Using the experimentally derived σ and α spatial profiles, linear constitutive relations coupled with conservation of charge and energy are used to model the cooling performance of the CG thin films. In comparison to their equivalent uniform conditions, the CG thin films yield higher cooling temperature ($\Delta T_c = T_H - T_c$) and higher coefficient of performance. The enhanced performance arises from efficient redistribution of the Joule heating and Peltier cooling effects. Moreover, the model calculations reveal that the magnitude of the σ profile and the slope of the α profile are specific attributes leading to the enhanced cooling in CG thin films. Overall, this study highlights a simple yet powerful strategy to improve the cooling performance of thermoelectric materials through functionally graded doped semiconducting polymers.

Thermoelectric (TE) systems have been a promising technology that interconverts heat and electrical energy.[1–6] TEs can be used for both energy harvesting by capturing waste heat as in thermoelectric generators and thermal energy management by controlling local temperature as in Peltier coolers. The efficiency of TE devices is characterized by its figure of merit, ZT, defined as $ZT = \alpha^2\sigma T/\kappa$, where σ is the electronic conductivity, α is the Seebeck coefficient, κ is the thermal conductivity, and T is the temperature in Kelvin.[1] Over the years, researchers have been focusing on enhancing the material's ZT to improve the performance of thermoelectric devices. Along with the effort on material optimization, the use of functionally graded materials (FGMs) offers alternative ways to further improve the device performance, especially in the case of Peltier coolers. FGMs are engineered materials whose properties are varied spatially either in a continuous or step-by-step (segmented) fashion throughout the volume of the material.[7–9] To date, implementing FGMs in Peltier cooling applications has been exclusively investigated with inorganic TE materials such as Bi_2Te_3 and PbTe.[9–14] In principle, functionally grading motifs with spatial variation in the thermoelectric properties enable more efficient redistribution of the Joule heating and Peltier cooling effects. This redistribution of heat leads to larger cooling temperature gradients and coefficient of performance (C.O.P.) compared to thermoelectric materials with uniform properties.[8,15–18] Importantly, modeling and simulations of inorganic FGMs as TE devices have been critical to elaborate optimal gradients in TE properties and establish the theoretical limits of cooling performance.[17,19–25] However, implementing the principles of functional grading using inorganic materials could be prohibitive as the fabrication and processing of conventional inorganic TE materials would require high temperature and pressure to achieve appropriate graded/segmented configurations.[8,10–12,26,27]

In contrast to inorganic-based materials, semiconducting-conjugated polymers with their inherent processability open the pathway for easier experimental methods of achieving FGMs. Together with solution and thermal processability, principles of molecular doping of semiconducting polymers control the carrier concentrations modulating thermoelectric properties.[28–31] In recent years, due to their

promising performance near room temperature, cooling ability of polymeric materials has been demonstrated to reveal the Peltier effect in organic thin film devices.[32–34] Particularly, in the case of thiophene-based semiconducting polymers, the addition of a molecular *p*-dopant such as a small organic acceptor (e.g., F4TCNQ, 2,3,5,6-tetrafluoro-7,7,8,8-tetracyanoquinodimethane) leads to electron transfer between the host polymer and dopant molecule, which modulates the carrier concentration, and therefore tuning the thermoelectric properties.[35,36] In our prior work, we showcased the first report on organic FGM for thermoelectrics by first casting a thin film of poly[2,5-bis(3-tetradecylthiophen-2-yl) thieno [3,2-b]thiophene] (PBTTT) and then infiltrating with F4TCNQ via the vapor doping method.[37] By using a home-built vapor doping apparatus, we were achievable a macroscopic double segmented FGMs, where each segment was tuned to have different doping level. Our work showcased the facile fabrication and characterization of functionally graded polymer thin films for TE materials, which opened pathways for further development on more complex FGMs.

In this Letter, we report on continuously graded (CG) thin films relevant to improved thermoelectric (Peltier) cooling. Spatial compositional control of the molecular *p*-dopant F4TCNQ in semiconducting PBTTT yields 1D profiles in σ and α. Moreover, first principle calculations based on linear Onsager theory and conservation of charge and energy are used to model the cooling performance of using the experimentally derived σ and α spatial profiles to demonstrate the utility of the CG thin films.

CG thin films of PBTTT:F4TCNQ, i.e., samples that have an in-plane, 1D lateral compositional gradient in molecular doping, were fabricated through sequential vapor doping (Fig. 1). In the vapor doping process, a neat PBTTT thin film is spin coated prior to the addition of F4TCNQ. As reported previously, this process largely preserves the molecular and long-range order of the polymer thin film, resulting in higher σ compared to films made through the solution-mixing doping process.[35,38–40] Importantly, sequential vapor doping allows for a relatively simple approach in achieving doping gradients along the in-plane, lateral direction of the thin film. Figure 1(b) shows a schematic of our home-built apparatus for controlled vapor doping of polymer thin films in an argon atmosphere glovebox. We use a cover mask where the side facing the PBTTT thin film has a *ca.* 0.10° wedge grading angle that leaves a narrow gap between PBTTT thin film surface and the mask. This gap controls the mass flux of F4TCNQ to the thin film and, thus, controls the doping level gradient as a function of doping time.

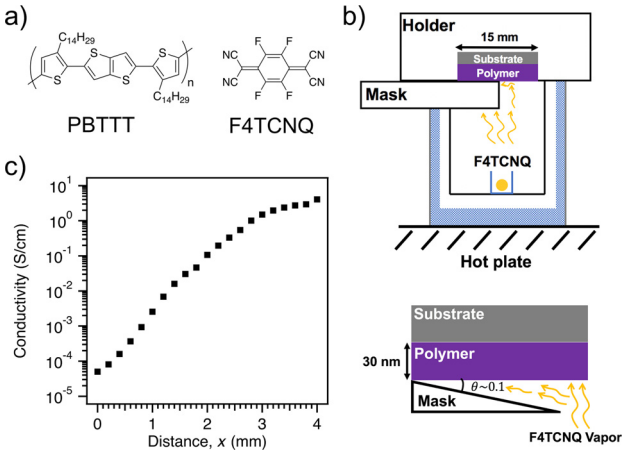

FIG. 1. (a) Chemical structures of the semiconducting polymer (PBTTT) and the molecular *p*-dopant (F4TCNQ). (b) Schematic drawing of setup used to vapor dope PBTTT with F4TCNQ to achieve continuously graded (CG) thin films. The bottom schematic highlights the small wedge grading angle (*ca.* 0.10°) of the cover mask, which controls the mass flux of F4TCNQ to the thin film, which allows for an in-plane, 1D lateral compositional gradient in doping. (c) 1D conductivity profile as a function of distance along the doping gradient for a representative CG thin film.

To first demonstrate the feasibility of this approach in achieving CG thin films, a neat PBTTT thin film (*ca.* 30 nm) was vapor doped by F4TCNQ with the cover mask using a doping time of 4 min (see the supplementary material, Fig. S1 and Table S1, for the correlation of doping time and doping level in PBTTT:F4TCNQ films).[37] Spatial distribution of σ for the resulting PBTTT:F4TCNQ thin film was measured through arrays of interdigitated electrodes (IDEs) across the dopant graded thin film in order to determine the presence of a continuous gradient in σ [Fig. 1(c)]. There are in total 20 IDEs, and each IDE measures a $100 \times 300\ \mu m^2$ region and is laterally spaced apart by 200 μm, thus measuring spatially across a total distance of 4 mm. This spatial distribution reveals the presence of a gradual gradient in σ, where σ increases across the graded region from the neat side to the doped side of the film.

To verify the gradient in σ arises from the compositional gradient of the dopant, grazing incidence wide angle X-ray scattering (GIWAXS) experiments were performed on a representative CG thin film. GIWAXS images of PBTTT:F4TCNQ neat to doped graded films are also shown in Fig. S2. The overall scattering patterns are qualitatively similar to neat PBTTT, which indicates that vapor infiltration with F4TCNQ largely preserves the semicrystalline morphology of PBTTT and is consistent with previous reports.[35,37,41] By taking line-cuts along the out-of-plane and in-plane directions (Fig. S3), we can observe quantitative changes through the characteristic side chain stacking (d_{100}) and π–π stacking ($d_{\pi-\pi}$) distances measured from neat side of the film to the doped side. Starting from the neat side, $d_{100} = 2.05$ nm maintains this value within the first 2 mm. Then, we observe a gradual increase in d_{100} to 2.27 nm over a total of 4 mm distance until stabilizing at the doped side of the film [Fig. S4(a)]. As shown in Fig. S4(b), the spatial distribution $d_{\pi-\pi}$ shows similar trend but inversely correlated. These changes to d_{100} and $d_{\pi-\pi}$ arise from the dopant F4TCNQ anions residing within regions of the side chain domain where an expansion of d_{100} and compression $d_{\pi-\pi}$ are observed. Therefore, both spatial profiles of d_{100} and $d_{\pi-\pi}$ indicate a gradient in dopant distribution of *ca.* 4 mm, which correlate well with the gradient profile distance as observed in IDE conductivity measurements.

To explore different gradient profiles, we fabricated three CG thin films with varying magnitudes in gradient of both σ and α across a 4 mm distance. These different gradients were achieved by varying the vapor doing time in our fabrication process described above. The graded profiles of the three thin films are shown in Fig. 2 and are assigned CG1, CG2, and CG3. Both σ and α were spatially measured at four spots along the desired in-plane, lateral gradient direction (Fig. S5). The measured values of σ and α across CG thin films are summarized in Tables S2 and S3. As seen in Fig. 2, α follows a linear profile, whereas the conductivity follows an exponential trend (note the

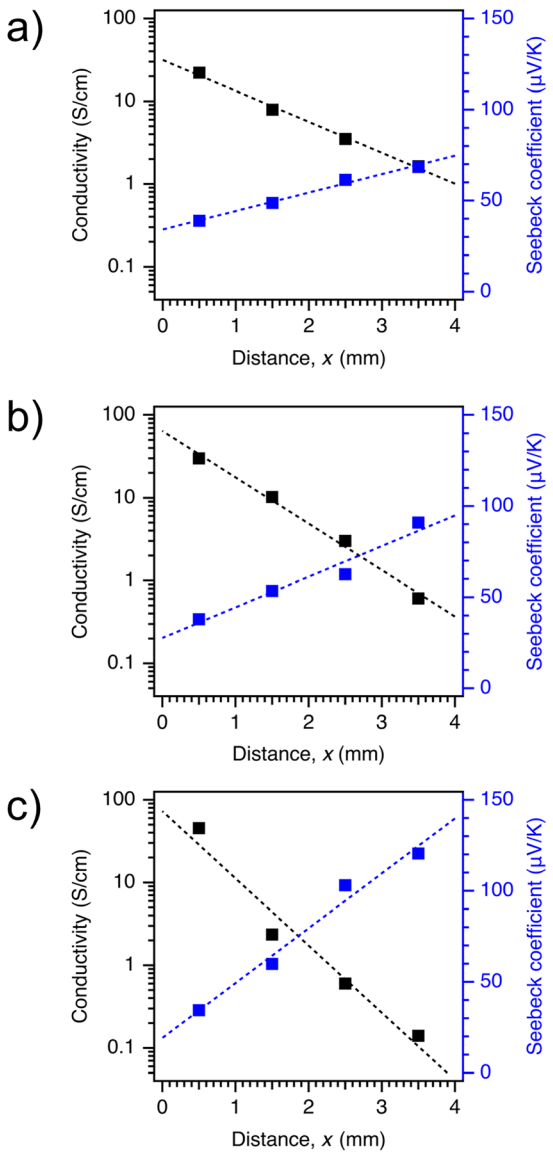

FIG. 2. Experimentally measured Seebeck coefficient (α, blue square) and conductivity (σ, black square) values along the 1D gradient distance, x, for three CG thin films exhibiting different extent of grading: (a) CG1, (b) CG2, and (c) CG3 thin films. The dashed lines represent fits to α and σ data from $x = 0$ to $x = 4$ mm. $\alpha(x)$ follows a linear profile, while $\sigma(x)$ follows an exponential profile (note log-scale on the plot). Fit values are summarized in Table I. In this profile, hot side (T_H) is set at $x = 4$, and the cold side (T_c) is set at $x = 0$.

log-scale of the conductivity axis). The spatial distribution in $\alpha(x)$ was fit to a linear equation [$\alpha(x) = kx + m$], and the spatial distribution in $\sigma(x)$ was fit to an exponential equation [$\sigma(x) = a\exp(bx)$], where k, m, a, and b have the unit of μV/mm K, μV/K, S/cm, and mm^{-1}, respectively. The fit values for these equations are provided in Table I and supplementary material. The slope of the $\alpha(x)$ profile increases from CG1 to CG3. As shown in the supplementary material, $\alpha(x)$ slopes are 10.1, 16.8, and 30.1 μV/mm K for CG1, CG2, and CG3, respectively. Moreover, the decay in $\sigma(x)$ profile increases from CG1 to CG3. The spatial averages of the conductivity (σ_{avg}) and Seebeck coefficient (α_{avg}) for CG thin film were calculated by integrating the gradient profile expressions across the total lateral distance (L) of 4 mm [Eqs. (S1) and (S2)]. The values for σ_{avg} and α_{avg} are provided in Table I. Here, these spatial average values were used to define an equivalent uniform (EU) condition for each corresponding experimentally derived CG thin film.

To better understand the utility of the experimentally derived CG profiles compared to their EU values, we modeled the cooling performance through first principle calculations based on linear Onsager theory and conservation of charge and energy.[42] Following the work of Seifert, Müller, and co-workers[17,22] the generalized constitutive equations for isotropic conditions are as follows:

$$\boldsymbol{j} = \sigma \boldsymbol{E} - \sigma\alpha\nabla T, \tag{1}$$

$$\boldsymbol{q} = \alpha T\boldsymbol{j} - \kappa\nabla T, \tag{2}$$

where, $\boldsymbol{j}$ is the current density, $\boldsymbol{E}$ is the electrical field, $\boldsymbol{q}$ is the heat flux, T is the temperature, σ is the electronic conductivity, α is the Seebeck coefficient, and κ is the thermal conductivity. Additionally, at steady-state conditions, conservation of charge and energy is as follows:

$$\nabla \cdot \boldsymbol{j} = 0, \tag{3}$$

$$\nabla \cdot \boldsymbol{q} = \boldsymbol{j} \cdot \boldsymbol{E}. \tag{4}$$

Based on the experimentally derived CG profiles, the constitutive equations can be reasonably simplified to model the case of 1D transport along the x-direction as shown in Eq. (5). More detailed derivation of this equation and explanation on contribution of the different heat fluxes in a Peltier cooler can be found in the supplementary material and Fig. S6

$$-\kappa\frac{\partial^2 T(x)}{\partial x^2} = \frac{j^2}{\sigma(x)} - j\frac{d\alpha(x)}{dx}T(x). \tag{5}$$

The term on the left-hand side of the equation ($-\kappa\frac{\partial^2 T(x)}{\partial x^2}$) refers to thermal conduction, the first term on the right-hand side ($\frac{j^2}{\sigma(x)}$) refers to Joule heating, and the second term on the right-hand side ($-j\frac{d\alpha(x)}{dx}T(x)$) refers to Peltier cooling. Importantly, the derivation of

TABLE I. Thermoelectric transport properties and model calculated cooling temperature (ΔT_c) of continuously graded (CG) PBTTT:F4TCNQ thin films.

CG thin film	$\sigma(x)$[a] (S/cm)	$\alpha(x)$[a] (μV/K)	σ_{avg} (S/cm)	α_{avg} (μV/K)	ΔT_c (K) $j = 3$ mA/mm^2	ΔT_c (K) C.O.P. $= 0.8$
CG1	$31.5\exp(-0.86x)$	$10.1x + 34.1$	3.58	54.4	0.75	10.5
CG2	$64.2\exp(-1.29x)$	$16.8x + 27.6$	1.92	61.2	1.64	9.78
CG3	$72.9\exp(-1.87x)$	$30.1x + 19.2$	0.308	79.4	12.8	3.51

[a]x is in mm.

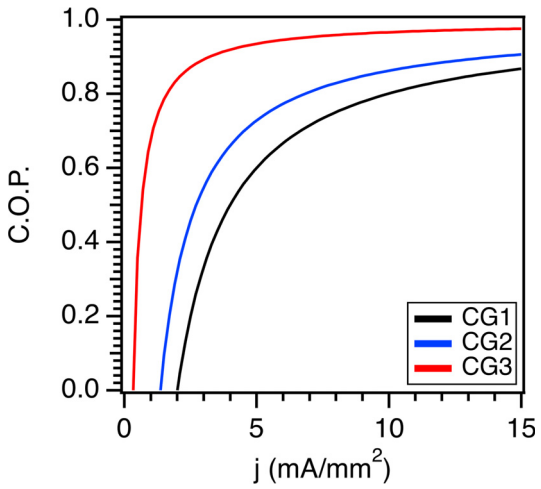

FIG. 3. Model calculated coefficient of performance (C.O.P.) using Eq. (6) for the CG thin films as a function of current density (j).

Eq. (5) assumes κ is constant across the length of the CG film where the composition of dopant varies. While such an assumption is valid for the range in doping levels used in this study based on the reported values of κ for PBTTT:F4TCNQ thin films,[43] it is important to note that other materials with higher doping levels and σ will need to account for the doping level dependence in κ.

Integration of Eq. (5) was performed to calculate the 1D temperature profile $T(x)$ at specific values of j for two cases: case 1: EU conditions where σ and α are spatially constant and case 2: CG profiles of $\sigma(x)$ and $\alpha(x)$. Note that T(x) is calculated assuming no heat transfer between the thin film and glass substrate. For case 1, Eq. (5) can be further simplified, and an analytical solution can be obtained (see the supplementary material for details). The values of σ and α when solving for case 1 were determined through spatial averaging of $\sigma(x)$ and $\alpha(x)$ [Eqs. (S1) and (S2)] as described earlier and reported in Table I. For case 2, the inclusion of the spatial dependence of $\sigma(x)$ and $\alpha(x)$ leads to non-linear differential equation requiring numerical integration of Eq. (5), which was done using custom Python code. For both cases, a mixed boundary condition was applied where the hot side T_H $(x = L)$ is fixed to 300 K, and the heat flux on the hot side is constant. Upon determining the T(x) profile, the cooling temperature, ΔT_c, is calculated from T_H minus the resulting temperature at the cold side $[T_C = T\,(x = 0)]$.

To calibrate for the range of j values in determining $T(x)$ and ΔT_c, the coefficient of performance (C.O.P.) was calculated using the gradient profiles of the CG thin films. C.O.P. is a metric used for cooling efficiency and is defined as the cooling power (absorbed heat per time per cross-sectional area) divided by the net power input density (electrical power input per cross-sectional area):

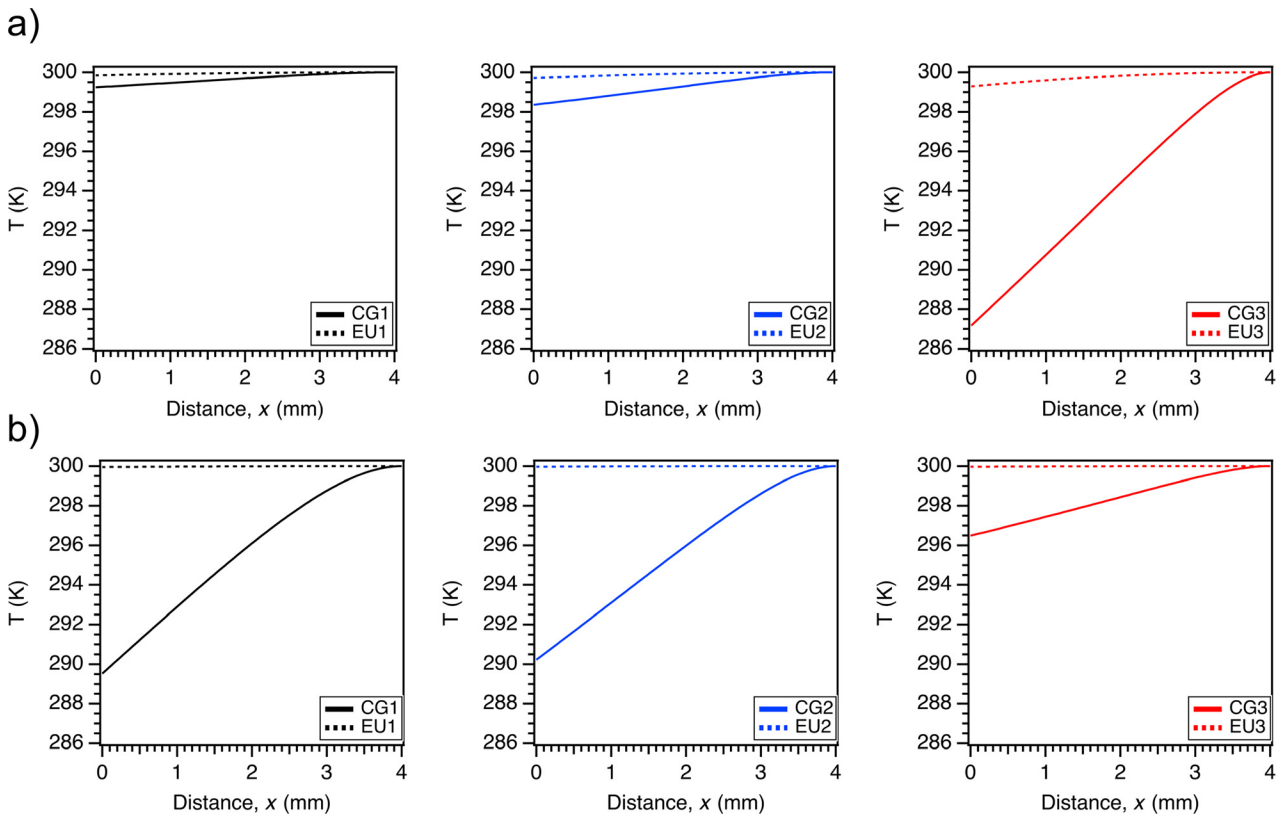

FIG. 4. Temperature profiles, $T(x)$, for the three continuously graded (CG) thin films and their corresponding equivalent uniform (EU) condition at (a) constant j of 3 mA/mm^2 and (b) constant C.O.P. of 0.80. The hot side ($T_H = 300$ K) is at $x = 4$, and the cold side (T_c) is at $x = 0$.

$$C.O.P. = \frac{\left[\alpha(x)T(x)j - \kappa\frac{\partial T(x)}{\partial x}\right]_{x=0}}{\int_0^L \left[\alpha(x)j\frac{\partial T(x)}{\partial x} + \frac{j^2}{\sigma(x)}\right]dx}, \quad (6)$$

where L is the length of the CG profile (4 mm). Note that Eq. (6) is specific to materials with a linear spatial gradient in TE properties. In comparison to the C.O.P. of a uniform material [Eq. (7)], the Joule heating term in the numerator is eliminated at the cold side due to the distributed Joule heating effect. In Fig. 3, C.O.P. of the three CG thin films is plotted against j. The value of j is within a reasonable range as the absolute current is on the order of μA, which is unlikely to cause any damage to the thin films. For all CG thin films, shape of the C.O.P. curve is similar, where it increases and plateaus at higher j. For example, at $j = 3$ mA/mm^2, the C.O.P. is 0.35, 0.55, and 0.89 for CG1, CG2, and CG3, respectively. Overall, CG3 yields the highest C.O.P. across the full range of j.

For comparison, the C.O.P. of conventional materials with uniform properties can be calculated through the following equation:

$$C.O.P. = \frac{\alpha T_C j - \frac{1}{2}j^2\frac{L}{\sigma} - \kappa\frac{\Delta T}{L}}{\alpha j\Delta T + j^2\frac{L}{\sigma}}. \quad (7)$$

As shown in Fig. S7 for the EU conditions, the C.O.P. profile show a different trend where C.O.P. decreases with j until reaching negative values. Note that for the uniform case, the Joule heating term ($\frac{1}{2}j^2\frac{L}{\sigma}$) increases more rapidly than the Peltier effect term ($\alpha T_C j$), which will eventually lead to a negative C.O.P. value at higher j (at 0.2 mA/mm^2 for EU3). Meaning that the applied electrical current is producing more heat than the heat being pumped by the Peltier effect, which leads to a net temperature increase. The transition to negative C.O.P. highlights the limited utility of the EU thin films based on the calculated σ_{avg} and α_{avg}. The difference in C.O.P. behavior between the CG and EU conditions illustrates an advantage for FGMs, where the redistributed Joule heating and Peltier cooling allow for a wider operational range of high efficiency.

The model calculated $T(x)$ and ΔT_c were determined upon integrating Eq. (5) for two cases: (1) $j = 3.0$ mA/mm^2 and (2) C.O.P. = 0.80. $T(x)$ profiles of CG and EU conditions are shown in Fig. 4, and the corresponding ΔT_c is shown in Fig. 5 and summarized in Table I. It is clear the EU condition exhibits negligible cooling for both cases, where, for example, ΔT_c is 0.15, 0.29, and 0.71 K at $j = 3.0$ mA/mm^2 for EU1, EU2, and EU3, respectively. On the other hand, all three CG thin films yield marked improvement in cooling. Compared to the EU conditions, the $T(x)$ profile exhibits greater extent of curvature from the hot side to the cold side arising from improved heat pumping across the length of the gradient. At $j = 3.0$ mA/mm^2, ΔT_c of the CG thin films are 0.75, 1.64, and 12.8 K for CG1, CG2, and CG3, respectively. It is clear that CG3 profile leads to the highest ΔT_c. At a fixed C.O.P. = 0.80, the corresponding j is 10, 6.9, and 1.6 mA/mm^2 for CG1, CG2, and CG3, respectively. In turn, the resulting ΔT_c is 10.5 K for CG1, 9.8 K for CG2, and 3.5 K for CG3. The higher ΔT_c of CG1 and CG2 arises from the larger j providing more heat pumping power. Moreover, while ΔT_c of CG3 is lower at this condition, a higher ΔT_c can be achieved at comparatively lower j; for example, $\Delta T_c = 10.5$ K is achieved at $j = 2.7$ mA/mm^2 for CG3. It

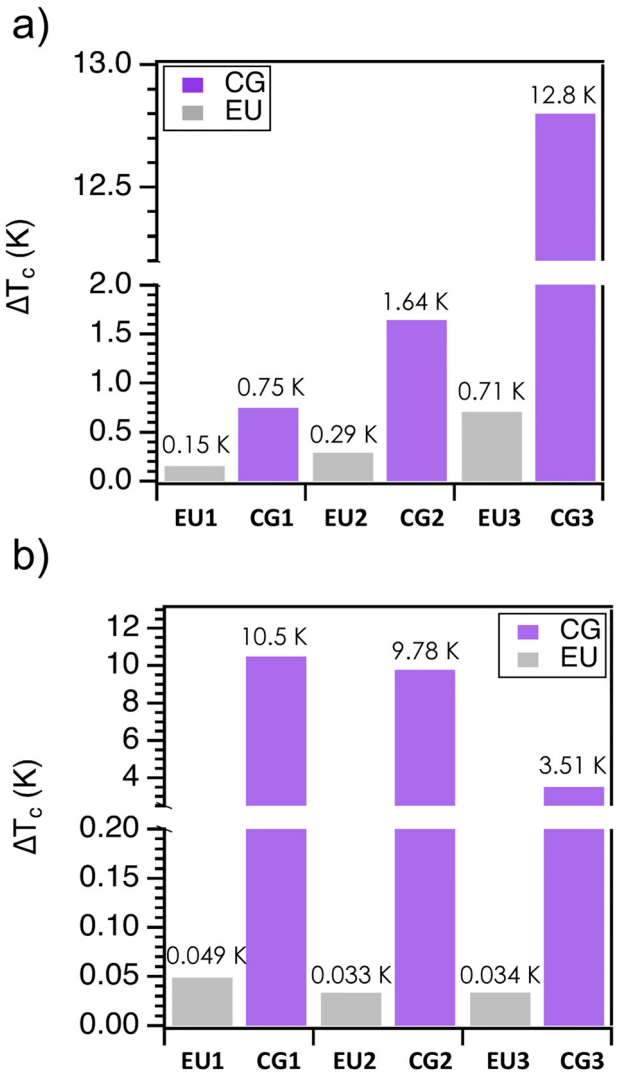

FIG. 5. Model calculated cooling temperatures ($\Delta T_c = T_H - T_c$) of continuously graded (CG) thin films and their equivalent uniform (EU) conditions at (a) constant current density (j) of 3 mA/mm^2 and (b) constant C.O.P. of 0.80.

should be noted that ΔT_c continues to increase with j for all CG thin films, especially CG3 (Fig. S8). This continuous increase in ΔT_c likely arises from the assumption in solving Eq. (5), where TE properties are independent of temperature and the application of a mixed boundary condition where the heat flux is constant at the hot side. One should take these ΔT_c values as the idealized upper bound in the cooling temperature. Overall, the results of the two conditions emphasize CG thin films allow for significant improvements in Peltier cooling and where the specific gradient profile of CG3 yields comparatively higher performance (more than an order of magnitude improvement in ΔT_c).

Analysis of the model-based calculations reveals important features of the $\sigma(x)$ and $\alpha(x)$ profiles leading to higher cooling temperature. Specifically, we compare the two extreme cases of CG1 and CG3. As seen from Eq. (5), the cooling temperature T(x) is strongly

dependent on $\sigma(x)$ and the spatial gradient of $\alpha(x)$, $\frac{d\alpha(x)}{dx}$. First, the exponential $\sigma(x)$ profile of CG3 has a higher σ at the cold side and a wider range in σ (72.9 S/cm at $x = 0$ to 0.0411 S/cm at $x = L$) compared to CG1 (31.5 S/cm at $x = 0$ to 1.01 S/cm at $x = L$). Additionally, the decay in σ is greater near the colder side for CG3 compared to CG1. These features in $\sigma(x)$ reduce the magnitude in Joule heating closer to the colder side. Second, the value of $\frac{d\alpha(x)}{dx}$ of the linear $\alpha(x)$ profile is higher for CG3 (30.1 μV/mm K) compared to CG1 (10.1 μV/mm K). This higher $\frac{d\alpha(x)}{dx}$ is an important characteristic to provide for a larger contribution from the Peltier effect term to offset the contribution from Joule heating. Finally, while the experimental validation of improved cooling is difficult with thin film system used in this study (see the supplementary material), future studies should consider alternative strategies with thicker films and full devices to demonstrate functional-grading cooling effect with sufficient power.

In summary, sequential vapor of PBTTT with F4TCNQ has been described as a straightforward approach of fabricating compositionally controlled continuously graded (CG) thin films. This approach leverages the inherent processibility of polymers and molecular dopants to yield various gradient profiles. In turn, we specifically fabricated three CG thin films with varying magnitudes in 1D gradient profiles of both σ and α across a 4 mm distance to explore how different gradient profiles control cooling performance. By applying model-based calculations through coupled energy and charge transport relations, we predicted the cooling temperature (ΔT_c) and coefficient of performance (C.O.P.) of the CG thin films compared to their equivalent uniform (EU) conditions. Specifically, CG3 profile leads to the highest ΔT_c of 12.8 K compared to 0.71 K for the corresponding EU condition. The enhancement in cooling arises from the magnitude of the σ profile and the slope of the α profile distinctive to the CG3 thin film. In turn, these features allow for efficient redistribution of the Joule heating and Peltier cooling to improve the cooling performance. Overall, this work together with our previous study[37] showcases that semiconducting polymers as FGMs are promising directions to further advance the development of more efficient organic thermoelectric devices.

See the supplementary material for details on the experimental methods, correlation of doping time and doping level, GIWAXS data and analysis, schematic of the contact geometry to spatially measure conductivity and Seebeck coefficient, tabulated conductivity and Seebeck coefficient values for continuously graded films, derivation of governing equations to determine the temperature profile for the uniform and continuously graded films, C.O.P. of the uniform equivalent films, and cooling temperature profiles at various input current density.

This work was supported by the University of Chicago Materials Research Science and Engineering Center, which is funded by National Science Foundation under Award No. DMR-2011854. This research used resources of the Advanced Photon Source, an Office of Science User Facility operated for the U.S. Department of Energy (DOE) by Argonne National Laboratory under Contract No. DE-AC02-06CH11357. Parts of this work were carried out at the Soft Matter Characterization Facility of the University of Chicago. This work made use of the Pritzker Nanofabrication Facility, which receives partial support from the SHyNE Resource, a node of the National Science Foundation's National Nanotechnology Coordinated Infrastructure (NSF ECCS-2025633). We thank Han Yang for useful discussion on cooling performance modelling.

DATA AVAILABILITY

The data that support the findings of this study are available from the corresponding author upon reasonable request.

REFERENCES

[1]G. J. Snyder and E. S. Toberer, Nat. Mater. **7**, 105 (2008).
[2]G. Snyder and T. Ursell, Phys. Rev. Lett. **91**, 148301 (2003).
[3]B. Russ, A. Glaudell, J. J. Urban, M. L. Chabinyc, and R. A. Segalman, Nat. Rev. Mater. **1**, 16050 (2016).
[4]Y. Wang, L. Yang, X.-L. Shi, X. Shi, L. Chen, M. S. Dargusch, J. Zou, and Z.-G. Chen, Adv. Mater. **31**, 1807916 (2019).
[5]I. Petsagkourakis, K. Tybrandt, X. Crispin, I. Ohkubo, N. Satoh, and T. Mori, Sci. Technol. Adv. Mater. **19**, 836 (2018).
[6]D. Beretta, N. Neophytou, J. M. Hodges, M. G. Kanatzidis, D. Narducci, M. Martin-Gonzalez, M. Beekman, B. Balke, G. Cerretti, W. Tremel, A. Zevalkink, A. I. Hofmann, C. Müller, B. Dörling, M. Campoy-Quiles, and M. Caironi, Mater. Sci. Eng.: R **138**, 100501 (2018).
[7]Z. Liu, M. A. Meyers, Z. Zhang, and R. O. Ritchie, Prog. Mater. Sci. **88**, 467 (2017).
[8]E. Müller, Č. Drašar, J. Schilz, and W. Kaysser, Mater. Sci. Eng. A **362**, 17 (2003).
[9]D. Almasi, M. Sadeghi, W. J. Lau, F. Roozbahani, and N. Iqbal, Mater. Sci. Eng. C **64**, 102 (2016).
[10]E. M. J. Hedegaard, A. A. H. Mamakhel, H. Reardon, and B. B. Iversen, Chem. Mater. **30**, 280 (2018).
[11]Q. Zhang, J. Liao, Y. Tang, M. Gu, C. Ming, P. Qiu, S. Bai, X. Shi, C. Uher, and L. Chen, Energy Environ. Sci. **10**, 956 (2017).
[12]N. Z. I. M. Sallehin, N. M. Yatim, and S. Suhaimi, AIP Conf. Proc. **1972**, 030003 (2018).
[13]V. L. Kuznetsov, L. A. Kuznetsova, A. E. Kaliazin, and D. M. Rowe, J. Mater. Sci. **37**, 2893 (2002).
[14]C. Kim, D. H. Kim, J. S. Kim, Y. S. Han, J. S. Chung, and H. Kim, J. Alloys Compd. **509**, 9472 (2011).
[15]E. Müller, K. Zabrocki, C. Goupil, G. J. Snyder, and W. Seifert, in *Materials, Preparation, and Characterization in Thermoelectrics*, edited by D. M. Rowe (CRC Press, 2012), pp 46–81.
[16]W. Seifert, E. Müller, and S. Walczak, in *Proceedings of the International Conference on Thermoelectrics* (IEEE, 2006), p. 714.
[17]E. Müller, S. Walczak, and W. Seifert, Phys. Status Solidi **203**, 2128 (2006).
[18]C. L. Cramer, H. Wang, and K. Ma, J. Electron. Mater. **47**, 5122 (2018).
[19]Z. Bian and A. Shakouri, in *Proceedings of the International Conference on Thermoelectrics (ICT)* (IEEE, 2006), p. 264.
[20]Z. Bian, H. Wang, Q. Zhou, and A. Shakouri, Phys. Rev. B **75**, 245208 (2007).
[21]L. N. Vikhor and L. I. Anatychuk, Appl. Therm. Eng. **26**, 1692 (2006).
[22]W. Seifert, M. Ueltzen, and E. Müller, Phys. Status Solidi A **194**, 277 (2002).
[23]E. Thiébaut, C. Goupil, F. Pesty, Y. D'Angelo, G. Guegan, and P. Lecoeur, Phys. Rev. Appl. **8**, 064003 (2017).
[24]Z. H. Jin and T. T. Wallace, J. Electron. Mater. **44**, 1444 (2015).
[25]L. Shen, W. Zhang, G. Liu, Z. Tu, Q. Lu, H. Chen, and Q. Huang, Appl. Therm. Eng. **168**, 114852 (2020).
[26]E. Hazan, O. Ben-Yehuda, N. Madar, and Y. Gelbstein, Adv. Energy Mater. **5**, 1500272 (2015).
[27]L. T. Hung, N. Van Nong, G. J. Snyder, M. H. Viet, B. Balke, L. Han, E. Stamate, S. Linderoth, and N. Pryds, Energy Convers. Manage. **99**, 20 (2015).
[28]R. Kroon, D. A. Mengistie, D. Kiefer, J. Hynynen, J. D. Ryan, L. Yu, and C. Müller, Chem. Soc. Rev. **45**, 6147 (2016).
[29]Q. Zhang, Y. Sun, W. Xu, and D. Zhu, Macromolecules **47**, 609 (2014).
[30]V. Vijayakumar, Y. Zhong, V. Untilova, M. Bahri, L. Herrmann, L. Biniek, N. Leclerc, and M. Brinkmann, Adv. Energy Mater. **9**, 1900266 (2019).

[31]I. Salzmann, G. Heimel, M. Oehzelt, S. Winkler, and N. Koch, Acc. Chem. Res. **49**, 370 (2016).
[32]W. Jin, L. Liu, T. Yang, H. Shen, J. Zhu, W. Xu, S. Li, Q. Li, L. Chi, C. Di, and D. Zhu, Nat. Commun. **9**, 3586 (2018).
[33]Z. Sun, J. Li, and W.-Y. Wong, Macromol. Chem. Phys. **221**, 2000115 (2020).
[34]Y. Sun, C.-A. Di, W. Xu, and D. Zhu, Adv. Electron. Mater. **5**, 1800825 (2019).
[35]S. N. Patel, A. M. Glaudell, K. A. Peterson, E. M. Thomas, K. A. O'Hara, E. Lim, and M. L. Chabinyc, Sci. Adv. **3**, e1700434 (2017).
[36]J. E. Cochran, M. J. N. Junk, A. M. Glaudell, P. L. Miller, J. S. Cowart, M. F. Toney, C. J. Hawker, B. F. Chmelka, and M. L. Chabinyc, Macromolecules **47**, 6836 (2014).
[37]T. Ma, B. X. Dong, G. L. Grocke, J. Strzalka, and S. N. Patel, Macromolecules **53**, 2882 (2020).
[38]E. Lim, K. A. Peterson, G. M. Su, and M. L. Chabinyc, Chem. Mater. **30**, 998 (2018).
[39]I. E. Jacobs, E. W. Aasen, J. L. Oliveira, T. N. Fonseca, J. D. Roehling, J. Li, G. Zhang, M. P. Augustine, M. Mascal, and A. J. Moulé, J. Mater. Chem. C **4**, 3454 (2016).
[40]D. T. Scholes, S. A. Hawks, P. Y. Yee, H. Wu, J. R. Lindemuth, S. H. Tolbert, and B. J. Schwartz, J. Phys. Chem. Lett. **6**, 4786 (2015).
[41]V. Vijayakumar, E. Zaborova, L. Biniek, H. Zeng, L. Herrmann, A. Carvalho, O. Boyron, N. Leclerc, and M. Brinkmann, ACS Appl. Mater. Interfaces **11**, 4942 (2019).
[42]L. Onsager, Phys. Rev. **37**, 405 (1931).
[43]O. Zapata-Arteaga, A. Perevedentsev, S. Marina, J. Martin, J. S. Reparaz, and M. Campoy-Quiles, ACS Energy Lett. **5**, 2972 (2020).